AJNR

This information is current as of May 19, 2025.

Demonstration of the Medullary Lamellae of the Human Red Nucleus with High-resolution Gradient-echo MR Imaging

Yonglin Pu, Yijun Liu, Jinwen Hou, Peter T. Fox and Jia-Hong Gao

Demonstration of the Medullary Lamellae of the Human Red Nucleus with High-resolution Gradient-echo MR Imaging

Yonglin Pu, Yijun Liu, Jinwen Hou, Peter T. Fox, and Jia-Hong Gao

BACKGROUND AND PURPOSE: **The human red nucleus is not a uniform structure. It is composed of caudally located magnocellular and rostrally located parvicellular subnuclei. In fact, the latter forms the bulk of the human red nucleus and can be subdivided histologically by two medullary lamellae into three parts. Because iron is deposited in the human red nucleus and gradient-echo sequences are more sensitive than spin-echo sequences in the detection of iron, a high-resolution gradient-echo MR sequence was used in this study to determine whether the medullary lamellae of the normal human red nucleus could be detected in vivo.**

METHODS: **Ten healthy volunteers (seven men and three women, 27–48 years old) were examined with a high-resolution T2*-weighted gradient-echo MR sequence using a 1.9-T MR imager. The scanning parameters were 60/40/15 (TR/TE/excitations) with a flip angle of 20°, a pixel size of 1 × 1 mm, and a slice thickness of 5 mm.**

RESULTS: **The medullary lamellae were depicted in all subjects in three imaging planes: coronal, oblique axial, and oblique sagittal. The signal intensity of the lamellae was consistently higher than that of other parts of the red nucleus on all images. With the lamellae, the parvicellular subnucleus of the human red nucleus can be divided into its subdivisions.**

CONCLUSION: **High-resolution gradient-echo MR imaging is capable of depicting the medullary lamellae of the normal human red nucleus in vivo.**

Histologically, the parvicellular subnucleus of the human red nucleus can be divided into three parts by medullary lamellae: the pars oralis, the pars dorsomedialis, and the pars caudalis (1) (Figs 1 and 2). Anatomic sections of the human brain have also shown the presence of lamellae in the red nucleus (2). Since various bands of fibers (fibers of the fasciculus retroflexus, rootlets of the oculomotor nerve, and fibers of the superior cerebellar peduncle) pass through the red nucleus (3, 4), it has been proposed that these myelinated fiber bundles constitute the lamellae (1). In addition, previous studies, using histochemical methods, have shown inhomogeneous deposition of iron in high concentration in the human red nucleus (5). The nucleus itself has higher iron content than its surrounding neural fibers. However, previous MR studies, using conventional spin-echo sequences,

have shown the human red nucleus as a uniformly hypointense area on both T1- and T2-weighted images (6, 7). To the best of our knowledge, the medullary lamellae in the red nucleus have not previously been demonstrated by means of a noninvasive imaging technique. Because the gradient-echo sequence is more sensitive than the spin-echo sequence in the detection of susceptibility changes induced by iron (8), a susceptibility sensitive high-resolution gradient-echo MR sequence was used in this study to determine whether the medullary lamellae of the normal human red nucleus could be detected in vivo.

Anatomy and Histology

Human red nuclei are a pair of globular structures located in the midbrain and can be divided into the caudally located magnocellular and rostrally located parvicellular subnuclei (3). From comparative neuroanatomic studies, it is known that the former is strongly developed in lower mammals, becomes less predominant among the apes, and in humans is only rudimentary. Indeed, there are only a few magnocellular neurons in the human red nucleus (1). They are gathered largely into two categories, the dorsomedial and the ventral

FIG 1.   *A,* Cross section through the mesencephalon at the level of the red nucleus shows the subdivision of the parvicellular subnucleus into the pars oralis and pars dorsomedialis (Heidenhain stain; original magnification × 8).
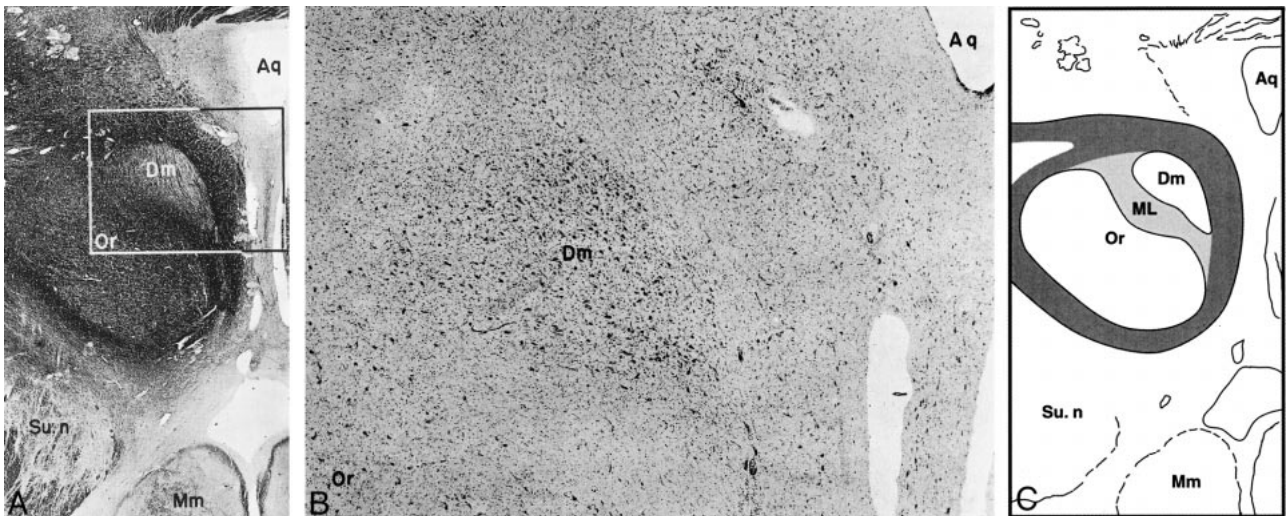
B, Cross section through the mesencephalon at the level of the red nucleus shows the subdivision of the parvicellular subnucleus into the pars oralis and pars dorsomedialis (original magnification × 30). The corresponding area of the adjacent myelin-stained section is delineated by the *square* in *A.*

C, Drawing of red nucleus partitions according to *A* shows the medullary lamella (*ML*) in the middle of the parvicellular subnucleus of the red nucleus.

Aq indicates sylvian aqueduct; *Dm,* pars dorsomedialis; *Or,* pars oralis; *Mm,* mammillary body; *Su.n,* substantia nigra. Parts *A* and *B* were reproduced with permission from S. Karger, Basel, Switzerland.

FIG 2.   *A,* Sagittal section through the mesencephalon at the level of the red nucleus shows the subdivision of the parvicellular subnucleus into the pars oralis, pars dorsomedialis, and pars caudalis (Heidenhain stain; original magnification × 8).
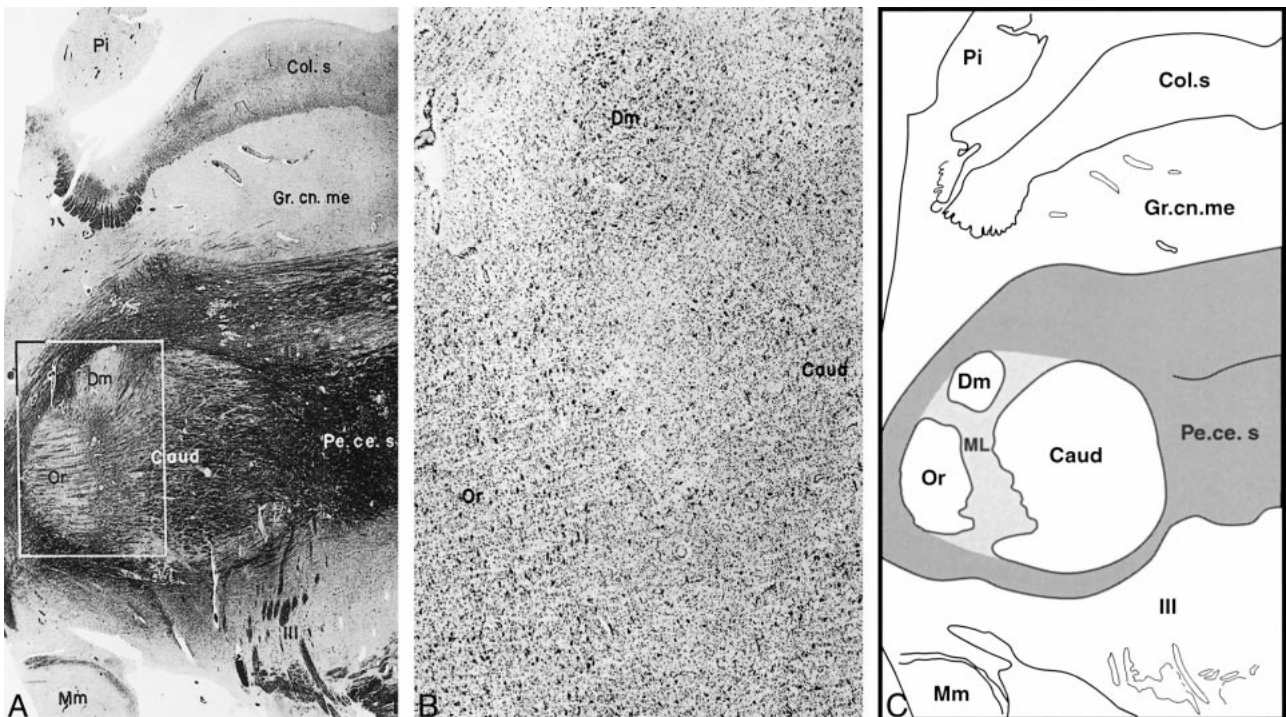
B, Sagittal section through the mesencephalon at the level of the red nucleus shows the subdivision of the parvicellular subnucleus into the pars oralis, pars dorsomedialis, and pars caudalis (original magnification × 30). The corresponding area of the adjacent myelin-stained section is delineated by the *square* in *A.*

C, Drawing of red nucleus partitions according to *A* shows the medullary lamellae (*ML*) in the middle of the parvicellular subnucleus of the red nucleus.

Dm indicates pars dorsomedialis; *Or,* pars oralis; *Caud,* pars caudalis; *Mm,* mammillary body; *Pe.ce.s,* pedunculus cerebellaris superior; *Pi,* pineal body; *III,* rootlet of the oculomotor nerve; *Col.s,* colliculus superior; *Gr. cn.me,* griseum centrale mesencephli. Parts *A* and *B* were reproduced with permission from S. Karger, Basel, Switzerland.
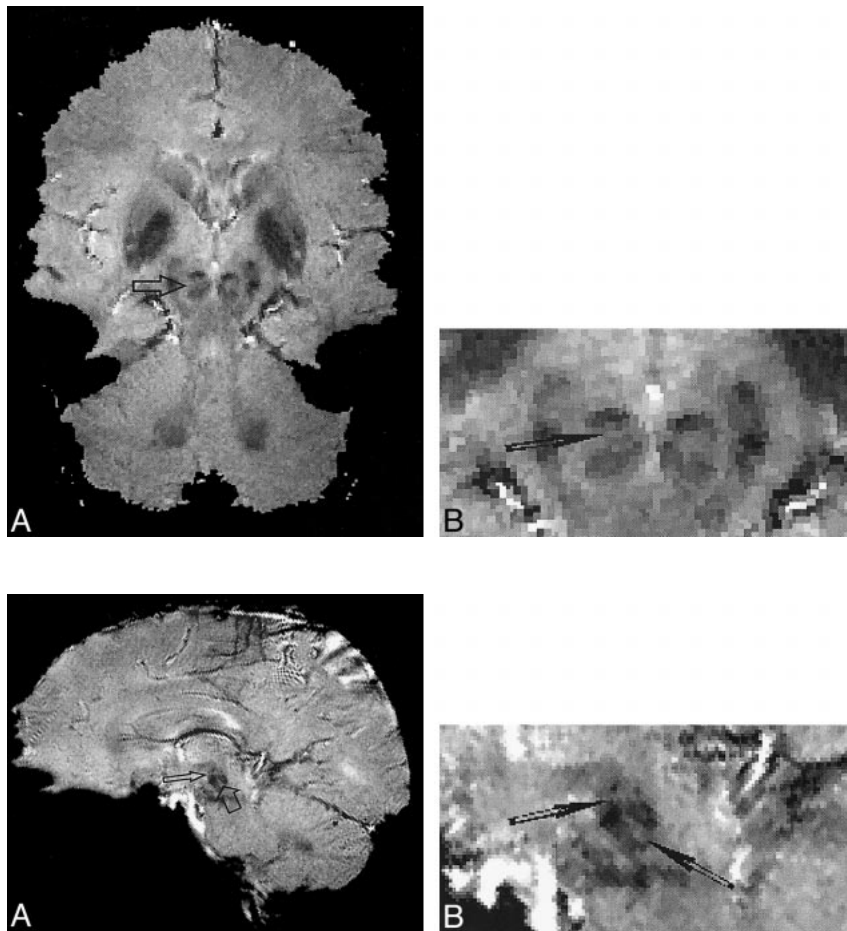
FIG 3. *A,* Typical oblique axial gradient-echo MR image (60/40/15) for one subject through the centers of the red and dentate nuclei of both sides. A lamella (*arrow*) within the red nuclei of both sides is clearly shown. It is triangular in shape with the apex directed medially. The signal intensity of the lamella is relatively higher than that of the other parts of the red nucleus.

B, Enlarged view of the red nuclei. *Arrow* indicates the medullary lamella.
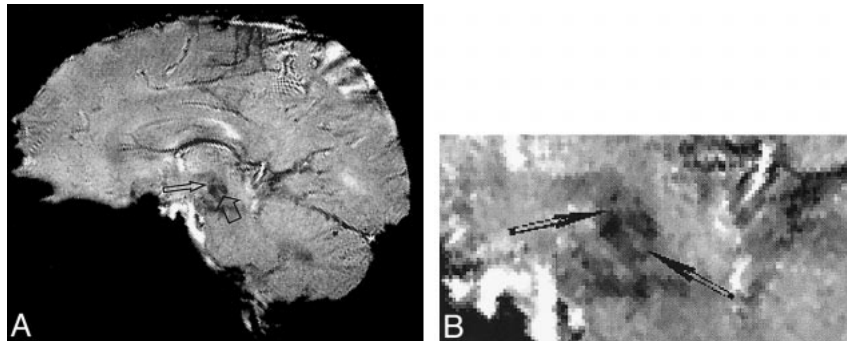

FIG 4. *A,* Typical oblique sagittal gradient-echo MR image (60/40/15) for one subject through the centers of the right red and dentate nuclei. Two lamellae (*arrows*) within the right red nucleus are clearly shown as cross-shaped structures. The signal intensity of the lamellae is relatively higher than that of the other parts of the red nucleus.

B, Enlarged view of the red nuclei. *Arrows* indicate the medullary lamellae.

groups, with an occasional single neuron scattered among the fibers of the superior cerebellar peduncle (1). On the other hand, the parvicellular subnucleus of the red nucleus is less developed in lower mammals, more pronounced among the apes, and finds its highest development in humans. It forms the bulk of the human red nucleus and can be subdivided histologically by two medullary lamellae into three parts: the pars oralis, the pars dorsomedialis, and the pars caudalis (1, 3, 4). On coronal and cross-sectional anatomic and histologic specimens, only one medullary lamella is visible in the red nucleus. On sagittal sections of histologic specimens, two medullary lamellae are visible (1, 2) (Figs 1 and 2). At the level of the habenulo-interpeduncular tract, the cells composing the oro-dorsomedial aspect of the red nucleus (pars dorsomedialis) are separated from the rest of the nucleus by a band of medullary lamella. A second lamella isolates the cells that form the oral pole of the red nucleus (ie, the pars oralis) from the more caudally situated pars dorsomedialis and pars caudalis.

Methods

MR images were acquired in 10 healthy subjects (seven men and three women, 27–48 years old) with a 1.9-T MR imager. The subjects had no history of neurologic or psychiatric illness and were recruited on a voluntary basis. Written consent was obtained from each subject after the MR procedures had been explained. To minimize motion artifacts, each subject's head was restrained in an individually molded plastic facial mask. In seven subjects, red nuclei were imaged in the oblique axial and oblique sagittal planes. The oblique axial sections were through the centers of the midbrain red nuclei and cerebellar dentate nuclei of both sides. The right oblique sagittal sections were through the centers of the right midbrain red nucleus and right cerebellar dentate nucleus. The left oblique sagittal section was through the centers of the left midbrain red nucleus and the left cerebellar dentate nucleus. In the other three subjects, the red nuclei were imaged coronally through the center of the red nuclei. The coronal section was parallel to the long axis of the brain stem. A T2*-weighted gradient-echo sequence with second-order motion compensation was used. The scanning parameters were 60/40/15 (TR/TE/excitations) with a flip angle of 20°, a matrix size of 200 × 200, a field of view of 20 × 20 cm, a pixel size of 1 × 1 mm, and a slice thickness of 5 mm. The bandwidth was 39 Hz, and total sampling time in readout direction was 25.6 milliseconds.

Results

Oblique Axial Images

On oblique axial images, the horizontal lamella was seen in all seven subjects in whom axial images were obtained. It was centrally located in the red nucleus and had a signal intensity relatively higher than that of the other parts of the nucleus (Fig 3). It was triangular or rectangular in shape

Fig 5. *A,* Typical coronal gradient-echo MR image (60/40/15) for one subject through both red nuclei. A lamella (*arrow*) is clearly seen within the nuclei extending lateromedially throughout the red nucleus. The signal intensity of the lamella is relatively higher than that of the other parts of the red nucleus.

B, Enlarged view of the red nuclei. *Arrow* indicates the medullary lamella.
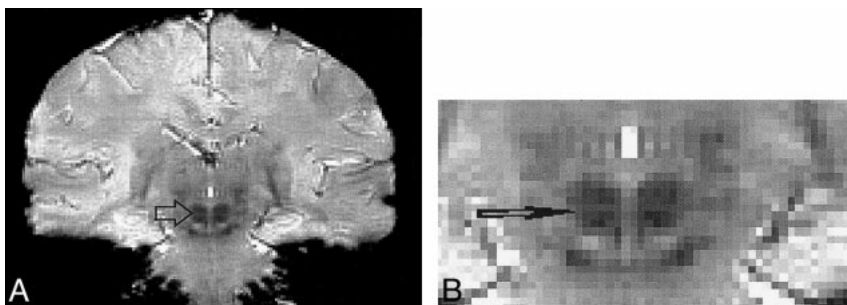
and spanned the entire nucleus lateromedially. The lamella divided the red nucleus into two parts: the oroventral and the caudodorsal sections.

Oblique Sagittal Images

On oblique sagittal images, two lamellae were seen in one of the red nuclei (Fig 4) in four of the seven subjects in whom sagittal images were obtained. In three subjects they were in the left red nucleus and in one they were in the right red nucleus. They were in the shape of a cross and located in the center of the red nucleus. The signal intensity of the lamellae was relatively higher than that of the other parts of the nucleus. The lamellae clearly divided the red nucleus into three parts: the rostral, caudoventral, and caudodorsal sections. In the red nucleus of the opposite side of the above-mentioned four subjects, and in both red nuclei of the other three remaining subjects, a single horizontal lamella was seen lying across the nucleus anteroposteriorly. This lamella clearly divided the red nucleus into two parts: the rostral and the caudal sections.

Coronal Images

The coronal images of all three subjects in whom coronal images were obtained showed a horizontal lamella. It was centrally located in the red nucleus and appeared as a horizontal band. The lamella divided the red nucleus into rostral and caudal parts. The signal intensity of the lamella was relatively higher than that of the other parts of the nucleus (Fig 5).

Discussion

Although the medullary lamellae in the human red nucleus has been studied histologically and anatomically (1, 2), they have not been detected with imaging methods in live humans. Previous MR studies of the human red nucleus with spin-echo sequences have not shown the presence of the medullary lamellae (6, 7).

The main advantage of a high-resolution gradient-echo MR sequence over a spin-echo sequence in mapping the iron distribution in the brain is its inherently higher sensitivity to the susceptibility effect induced by iron in the brain tissue (8). The

presence of iron in brain tissue may have three effects: a shift in the local resonance frequency because of iron-induced magnetic susceptibility, a decrease in the effective T2 relaxation time due to molecular diffusion through the susceptibility induced gradient, and a local line broadening due to the gradient within a voxel. Gradient-echo sequences map both irreversible T2 decay as well as spin dephasing caused by a broadened line width manifested by T2* decay. However, the spin-echo techniques only map the irreversible T2 decay, along with diffusion-related dephasing. The effects of static field variations within a voxel are refocused and thus do not affect the spin-echo signal intensity. Therefore, the gradient-echo technique should be more sensitive than the spin-echo technique in mapping iron concentration in the brain. The red nucleus and its medullary lamellae were clearly demonstrated by the gradient-echo sequence used in this study, because there is an iron concentration difference among the cellular parts and the medullary lamellae of the red nuclei and their surrounding neuronal fibers, as indicated by previous histochemical studies (5).

In this study, two medullary lamellae were seen on sagittal images of one of the red nuclei in four of seven subjects. In the other scanning planes, only one lamella was demonstrated in each of 10 subjects. These results are consistent with previous histologic and anatomic findings in human cadavers (1, 2). On sagittal images, a single lamella was shown in the red nucleus of the opposite side of the above-mentioned four subjects and in both the red nuclei of the remaining three subjects. The discrepancies between the MR findings in these subjects on sagittal images and those in a previous histologic study of human cadavers (1) may be explained by the partial volume averaging effect of MR imaging. If the MR imaging plane is parallel to the plane of the lamellae, MR imaging may fail to detect them because the voxels containing lamella tissue would also contain a significant amount of other nonlamella tissue. On the other hand, if the MR imaging plane is perpendicular to the lamella plane, MR imaging may detect the lamellae easily.

Detection of the medullary lamellae of the human red nucleus in live human subjects by neuroimaging techniques has potential clinical and research applications. First, the medullary lamellae

revealed by in vivo MR imaging may be used as internal anatomic landmarks to divide the parvicellular subnucleus of the human red nucleus into its subdivisions. This noninvasive technique of dividing the red nucleus may, in turn, help clinicians locate lesions of the red nucleus more precisely. In addition, the technique may be useful in helping to determine the functions of each segment of the human red nucleus in functional neuroimaging studies. Second, this detection of the lamellae may serve as a basis for the study of the nature and origin of the structures themselves by using sophisticated, newer MR techniques, such as diffusion-based fiber tract analysis (9), and by observing distal neuronal degeneration (10).

Conclusion

Our results show that high-resolution gradient-echo MR imaging is capable of demonstrating the medullary lamellae of the normal human red nucleus in vivo.

References

1. Olszewski J. *Cytoarchitecture of the Human Brain Stem.* Basel: Karger;1980;54–60, 132–135
2. Hanaway J, Woolsey TA, Gado MH, Roberts MP. *The Brain Atlas: A Visual Guide to the Human Central Nervous System.* Bethesda, Md: Fitzgerald Science Press;1998;68
3. Carpenter, MB. *Human Neuroanatomy.* 9th ed. Baltimore, MD: Williams & Wilkins;1996;549–552
4. Krieg WJ. *Functional Neuroanatomy.* 2nd ed. Bloomington, IL: Pantograph Printing;1966;309–318
5. Morris CM, Candy JM, Oakley AF, Bloxham CA, Edwardson JA. **Histochemical distribution of non-haem iron in the human brain.** *Acta Anat* 1992;144:235–257
6. Thomas LO, Boyko O, Anthony DC, Burger PC. **MR detection of brain iron.** *AJNR Am J Neuroradiol* 1993;14:1043–1048
7. Patel VH, Friedman L. *MRI of the Brain, Normal Anatomy and Normal Variants.* Philadelphia: Saunders;1997;161–173, 421–413
8. Wismer GL, Buxton RB, Rosen BR, et al. **Susceptibility induced MRI line broadening: applications to brain iron mapping.** *J Comput Assist Tomogr* 1988;12:259–265
9. Pierpaoli C, Jezzard P, Basser PJ, Barnett A, Di Chiro G. **Diffusion tensor MR imaging of human brain.** *Radiology* 1996;201:637–648
10. Rabin BM, Hebel DJ, Salamon-Murayama N, Russell EJ. **Distal neuronal degeneration caused by intracranial lesions.** *AJR Am J Roentgenol* 1998;171:95–102